Supporting Information

Gas transport properties of the Metal-Organic Framework (MOF) assisted Polymer of Intrinsic Microporosity (PIM-1) thin-film composite membranes

Elvin Aliyev[†], *Jan Warfsmann*[‡], *Begum Tokay*[‡], *Sergey Shishatskiy*[†], *Young-Joo Lee*[§], *Jelena Lillepaerg*[†], *Neil R. Champness*[‖], *Volkan Filiz*[*,†]

[†] Institute of Polymer Research, Helmholtz-Zentrum Geesthacht, Max-Planck Str. 1, 21502 Geesthacht, Germany

[‡] Department of Chemical and Environmental Engineering, Faculty of Engineering, University of Nottingham, University Park, NG7 2RD, Nottingham, UK

[§] Institute of Inorganic and Applied Chemistry, Department of Chemistry, University of Hamburg, Martin-Luther-King-Platz-6, 20146 Hamburg, Germany

[‖] School of Chemistry, University of Nottingham, University Park, NG7 2RD, Nottingham, UK

Corresponding Author

*E-mail address: volkan.filiz@hzg.de (Volkan Filiz)

CONTENT

Total number of pages: S1-S10

Total number of tables: S6

Total number of figures: S5, S7-S10

Characterization methods. Fourier transform infrared (FTIR) spectra were recorded in an attenuated total reflectance (ATR) mode on a Bruker ALPHA FT-IR spectrometer (Bruker, Ettlingen, Germany). The transmittance measurements were done at ambient temperature in a spectral range of 400–4000 cm $^{-1}$ with a resolution of 4 cm^{-1} and an average of 64 scans. Solid-state NMR experiments were carried out on a Bruker Avance II 400 spectrometer (Bruker, Rheinstetten, Germany) equipped with a 4 mm double resonance probe. Ramped polarization transfer with ^{13}C 90° pulse length of 4.2 μs, recycle delay of 3 s, and magic angle spinning rate of 14 kHz was used to acquire ^{13}C cross-polarization (CP) magic-angle spinning (MAS) NMR spectra. The thermal stability analysis of the samples was carried out on a Netzsch TG209 F1 Iris (Selb, Germany) for ZIF-7 and $Zn_2(bim)_4$ and a TA Instruments Q500 instrument for TIFSIX-3. ZIF-7 and $Zn_2(bim)_4$ samples were tested under argon flow (50 mL min^{-1}) from 25 °C to 800 °C at 5 K min^{-1}, while the thermal heating of TIFSIX-3 was up to 700 °C under air flow (100 mL/min) with a heating rate of 5 °C/min. A scanning electron microscope Merlin (Zeiss, Oberkochen, Germany) was used to characterize the ZIF-7 and $Zn_2(bim)_4$ particles and all the mixed matrix membranes of this work at an accelerating voltage of 1.3-3.0 kV. To suppress charging of the sample surfaces, they were coated with approx. 2 nm Pt using a sputter coating device MED 020 (Leica Microsystems, Wetzlar, Germany). GPC measurement was performed at room temperature in THF on a Waters instrument (Waters GmbH, Eschborn, Germany) using a refractive index detector and polystyrene polymer standards of different molecular weights (Polymer Labs GmbH). A D8 discover X-ray diffractometer (Bruker, Ettlingen, Germany) with Cu Kα radiation (λ = 1.54184 Å, 50 kV, 1000 mA) was applied for the XRD experiments of ZIF-7 and $Zn_2(bim)_4$ particles at a scanning rate of 1° min^{-1}. Air-tight sample holders (Bruker, Ettlingen, Germany) were used to prevent any contaminations of the samples. The simulated XRD patterns were done using the Match!3 software. For the nitrogen adsorption experiments, degassing of the samples was conducted at 80 °C for 1 h in the vacuum, and at 150 °C overnight in the vacuum (MIL-53) or at 100 °C in vacuum overnight (TIFSIX-3-Ni). Sample porosity and BET area were determined by N_2-adsorption via Micrometrics Tristar II-adsorber. N_2-isotherms were measured at 77 K. Surface area was calculated by BET-Theory using 7 data points between 0.05 and 0.28 P/Po.

Gas adsorption measurements. The gas adsorption analysis of the MOF nanoparticles was conducted on a magnetic suspension balance (MSB) (Rubotherm Series IsoSORP® sorption analyzer, TA® Instruments, New Castle, DE, USA) with an uncertainty of 10 µg. The sample of Mg-MOF-74 in powder form was evacuated at 120 °C for 24 h in order to remove the residual gas. The density of the sample was estimated in-situ with He at 30 °C with MSB in the pressure range from 10^{-5} bar to 50 bar. The adsorption measurements were conducted from high vacuum to 50 bar stepwise with an uncertainty of ± 0.1 % for CH_4, N_2, O_2, and CO_2 series. The specific uptake was analyzed considering the gas buoyancy series. The specific uptake was analyzed considering the gas buoyancy [1].

The equilibrium concentration C of gas in the polymer for a given gas pressure p was obtained from the equation:

$$C = \frac{C_H' \, b \, P}{1 + b \, P} \tag{S1}$$

where C'_H is the Langmuir sorption capacity related to addition sorption owing to the non-equilibrium volume, P is the pressure, and b is the Langmuir affinity parameter.

Gas separation measurements. After membrane casting, the samples of 20 mm in diameter were cut and placed into the measurement cell of the membrane testing facility, and gas transport properties for H_2, CH_4, N_2, O_2, and CO_2 were determined at 30 °C and 500 mbar feed pressure. The effective membrane area tested during the experiments was 0.97 cm^2. The feed pressure of a maximum 500 mbar and permeate pressure of maximum 10 mbar give one the possibility to consider all aforementioned gases as ideal for the calculation of the membrane permeance. During gas permeance experiments four stamps of each membrane were tested. The cycles of every single gas permeances through membranes were 20 (each tested gas passed through the membranes 20 times for getting better results). The gas permeation experimental facility is described elsewhere in detail [2]. The membrane permeance (L) of a gas can be calculated using the equation:

$$L=\frac{V\ 22.41\ 3600}{R\ T\ A\ t}\ln\frac{(P_F - P_0)}{(P_F - P_{P(t)})} \tag{S2}$$

where L is the gas permeance (m^3(STP) m^{-2} h^{-1} bar^{-1}), V is the permeate volume (m^3), 22.41 is the molar volume (m^3(STP) $kmol^{-1}$), 3600 is the time conversion factor, R is the ideal gas constant (0.08314 m^3 bar K^{-1} $kmol^{-1}$), T is the temperature (K), t is the time of measurement between permeate pressure points P_0 and $P_{P(t)}$ (s), A is the membrane area (m^2), and P_F, P_0 and $P_{P(t)}$ are the pressures at the feed, and the permeate side at the start and at the end time of measurement, respectively (mbar). The ideal selectivity for a gas pair A and B ($\alpha_{A/B}$) can be calculated by the equation:

$$\alpha_{A/B}=\frac{L_A}{L_B} \tag{S3}$$

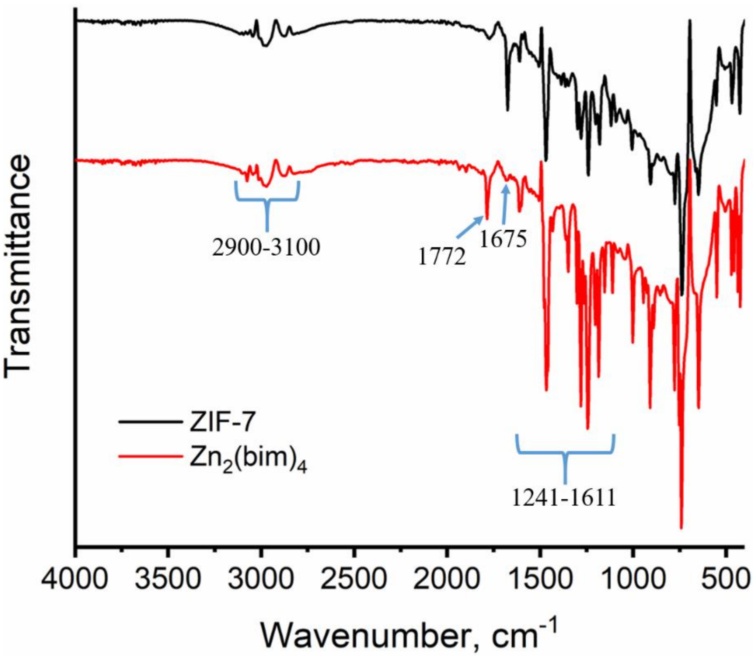

Figure S1. FTIR spectra of the synthesized ZIF-7 and $Zn_2(bim)_4$ particles.

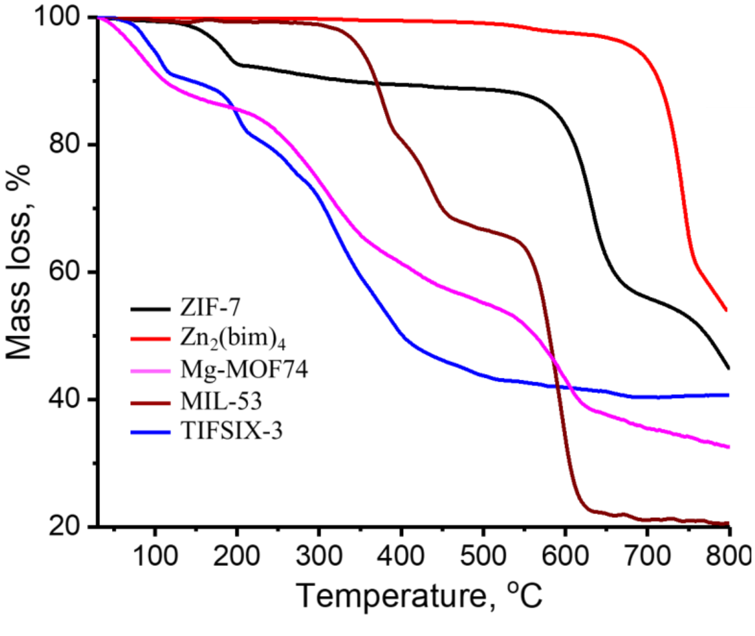

Figure S2. TGA analysis of the synthesized MOF nanoparticles.

Table S1. Permeability coefficients for the MOF containing PIM-1 TFC membranes.

Membrane code	Filler	Wt.% of filler	Permeability coefficients, Barrer					Ref.
			H_2	N_2	CH_4	CO_2	O_2	
Literature data								
PIM-1	-	-	1300	92	125	2300	370	[3]
PIM-1/UiO-66	UiO-66	9	3080	256	371	5940	1010	[4]
PIM-1/CAU-21-ODB	CAU-21-ODB	15	7295	186	-	-	-	[5]
PIM-1/ZIF-67	ZIF-67	20	3500	219	315	5200	-	[6]
Experimental data of current study[ǂ]								
PIM-1	-	-	670 ± 12	64 ± 20	102 ± 4	1350 ± 42	207 ± 6	This work
PIM1-$Zn_2(bim)_4$_2	$Zn_2(bim)_4$	2	792 ± 83	51 ± 8	73 ± 12	1000 ± 166	217 ± 32	
PIM1-$Zn_2(bim)_4$_10	$Zn_2(bim)_4$	10	1358 ± 74	129 ± 12	194 ± 12	1990 ± 100	436 ± 24	
PIM1-MOF74_8	Mg-MOF-74	8	1815 ± 281	112 ± 14	156 ± 20	1935 ± 235	464 ± 70	
PIM1-MOF74_10	Mg-MOF-74	10	1682 ± 224	114 ± 6	156 ± 4	1846 ± 139	445 ± 39	
PIM1-MIL53_4	MIL-53	4	1027 ± 354	56 ± 20	75 ± 20	953 ± 254	223 ± 80	
PIM1-TIFSIX3_4	TIFSIX-3	4	1010 ± 241	52 ± 16	71 ± 24	1000 ± 262	223 ± 67	

[ǂ] 10 wt.% of loadings of Mg-MOF-74 and $Zn_2(bim)_4$ particles are shown here as data for aging experiments.

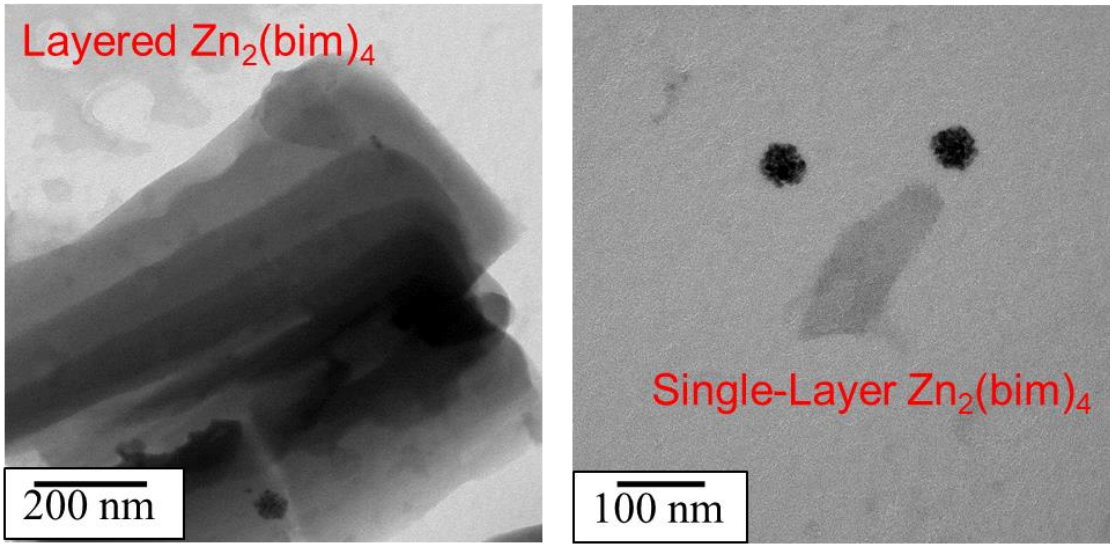

Figure S3. TEM images of layered $Zn_2(bim)_4$ and single-layer $Zn_2(bim)_4$ nanosheet after exfoliation. Two black spots in the right figure are coming from the carbon black support itself.

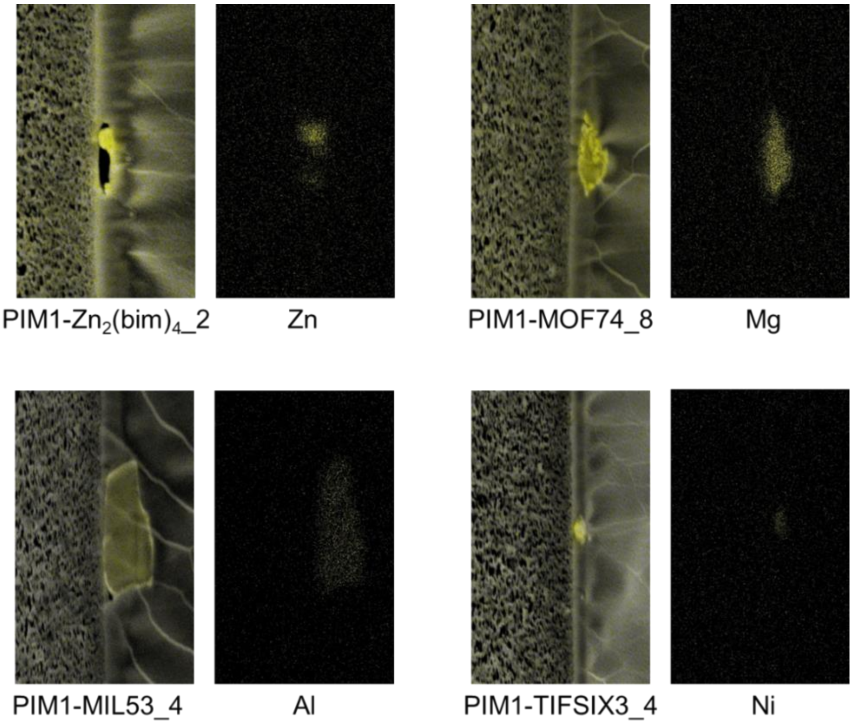

Figure S4. Cross-sectional EDX elemental mapping for the prepared thin-film composite membranes.

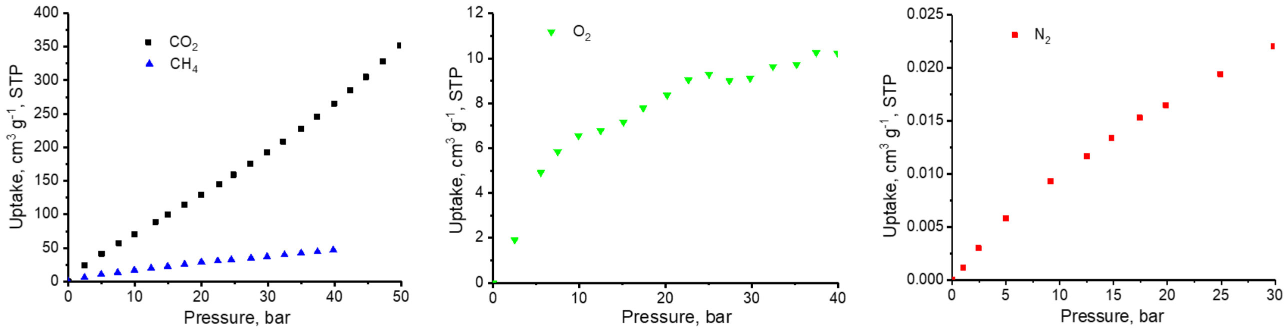

Figure S5. The experimental adsorption isotherms of CO_2, CH_4, O_2, and N_2 in pristine Mg-MOF-74.

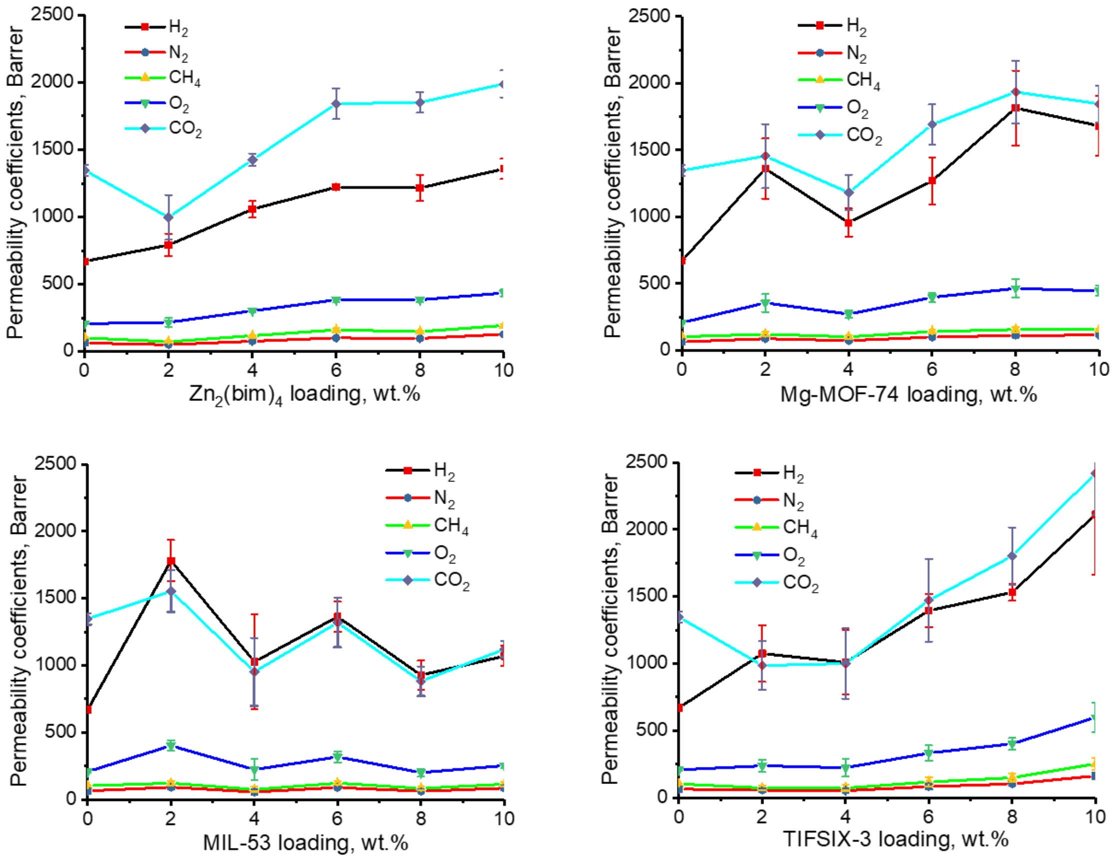

Figure S6. Gas permeability coefficients of different gases as a function of MOF content in PIM-1.

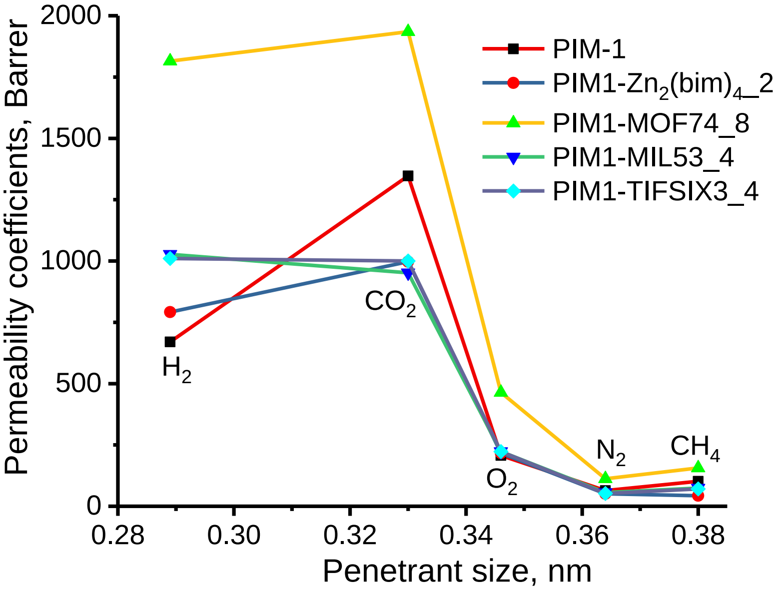

Figure S7. Gas permeability as a function of penetrant kinetic diameter for pure PIM-1 and MOF-incorporated PIM-1 mixed-matrix membranes.

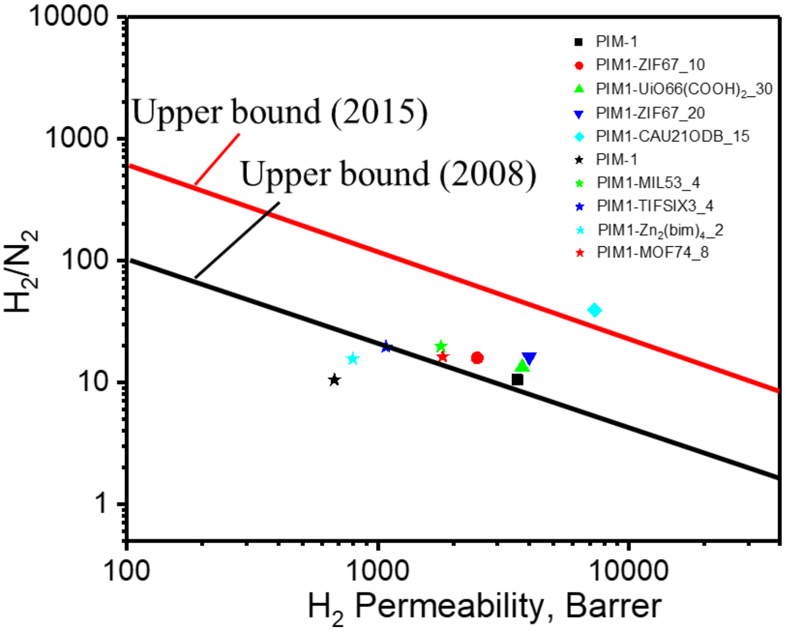

Figure S8. H_2 Permeability versus H_2/N_2 selectivity along with reported literature data. The results shown in “stars” represent the findings of the current work.

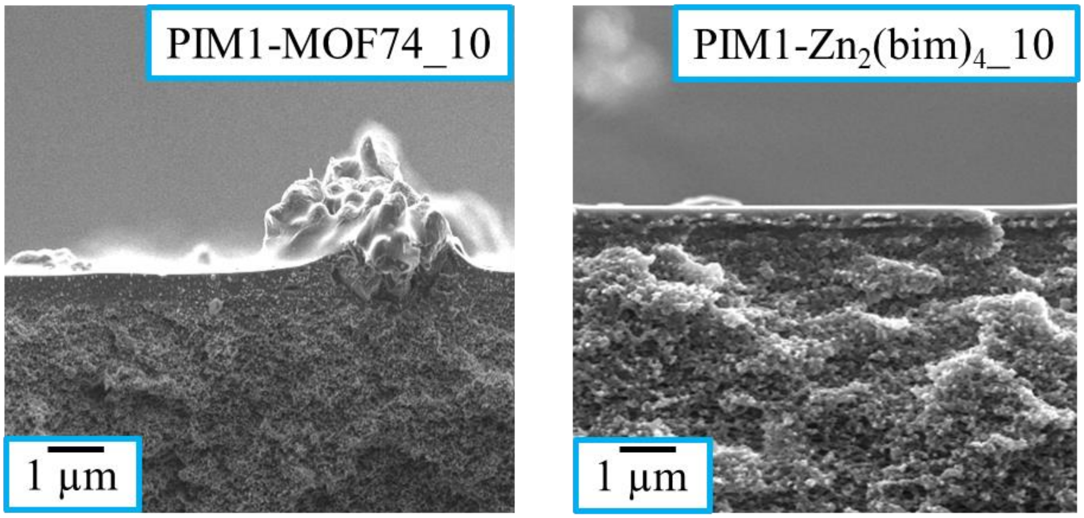

Figure S9. The SEM images of the MMMs of PIM-1 and Mg-MOF-74 (left), and PIM-1 and $Zn_2(bim)_4$ (right) particles used in long-term aging experiments.

REFERENCES

1. Aionicesei, E.; Škerget, M.; Knez, Ž., Measurement of CO2 solubility and diffusivity in poly(l-lactide) and poly(d,l-lactide-co-glycolide) by magnetic suspension balance. *The Journal of Supercritical Fluids* **2008,** *47* (2), 296-301, DOI: 10.1016/j.supflu.2008.07.011.

2. Car, A.; Stropnik, C.; Yave, W.; Peinemann, K.-V., Pebax®/polyethylene glycol blend thin film composite membranes for CO2 separation: Performance with mixed gases. *Separation and Purification Technology* **2008,** *62* (1), 110-117, DOI: 10.1016/j.seppur.2008.01.001.

3. Budd, P. M.; Msayib, K. J.; Tattershall, C. E.; Ghanem, B. S.; Reynolds, K. J.; McKeown, N. B.; Fritsch, D., Gas separation membranes from polymers of intrinsic microporosity. *Journal of Membrane Science* **2005,** *251* (1), 263-269, DOI: 10.1016/j.memsci.2005.01.009.

4. Khdhayyer, M. R.; Esposito, E.; Fuoco, A.; Monteleone, M.; Giorno, L.; Jansen, J. C.; Attfield, M. P.; Budd, P. M., Mixed matrix membranes based on UiO-66 MOFs in the polymer of intrinsic microporosity PIM-1. *Separation and Purification Technology* **2017,** *173*, 304-313, DOI: 10.1016/j.seppur.2016.09.036.

5. Zhang, C.; Liu, B.; Wang, G.; Yu, G.; Zou, X.; Zhu, G., Small-pore CAU-21 and porous PIM-1 in mixed-matrix membranes for improving selectivity and permeability in hydrogen separation. *Chemical Communications* **2019,** *55* (49), 7101-7104, DOI: 10.1039/C9CC02537E.

6. Wu, X.; Liu, W.; Wu, H.; Zong, X.; Yang, L.; Wu, Y.; Ren, Y.; Shi, C.; Wang, S.; Jiang, Z., Nanoporous ZIF-67 embedded polymers of intrinsic microporosity membranes with enhanced gas separation performance. *Journal of Membrane Science* **2018,** *548*, 309-318, DOI: 10.1016/j.memsci.2017.11.038.